JCARME
ISSN: 2228-7922
SRTTU
Journal of Computational and Applied Research in Mechanical Engineering
Vol. 6, No. 1, pp. 75- 89, Aut.-Win. 2016-17
http://jcarme.srttu.edu

A truly meshless method formulation for analysis of non-Fourier heat conduction in solids

Isa Ahmadi*

Advanced Materials and Computational Mechanics Lab., Department of Mechanical Engineering, University of Zanjan, P.O.Box: 45371-38791, *Zanjan, Iran*

Article info:
Received: 11/10/2015
Accepted: 03/04/2016
Online: 11/09/2016

Keywords:
Meshless method,
Non-fourier heat conduction,
Temperature waves,
Heat propagation,
Analytical solution.

Abstract
The non-Fourier effect in heat conduction is important in strong thermal environments and thermal shock problems. Generally, commercial FE codes are not available for analysis of non-Fourier heat conduction. In this study, a meshless formulation is presented for the analysis of the non-Fourier heat conduction in the materials. The formulation is based on the symmetric local weak form of the second-order non-Fourier heat conduction equation in terms of the temperature. Using the local weak form of heat transfer equations in the sub-domains, the governing equation of the non-Fourier heat conduction is discretized in the space domain to the second order ordinary differential equations for the time. The discretized equations are integrated into the time domain with an appropriate finite difference method. The fictitious numerical oscillations are completely suppressed from the front of temperature waves in the presented method. An analytical series solution is developed for the non Fourier heat transfer in one-dimensional heat transfer for special boundary conditions and the accuracy of presented numerical meshless method is validated by comparison of the results of the numerical meshless solution and the series solution. The numerical results are presented for non-Fourier heat conduction for various Vernotte numbers and boundary conditions and the results are compared with the results of the classical Fourier heat conduction.

Nomenclature

c^*: dimensionless speed
c: heat capacity ($J/kg/K$)
Fo: Fourier number
g: volumetric heat generation rate (W/m^3)
k: the coefficient of thermal conductivity ($W/m/K$)
$\boldsymbol{n}$: outward normal direction to the boundary Γ
q_i^*:dimensionless heat flux
q_i: heat flux (W/m^2)
$\bar{q}$: prescribed normal heat flux (W/m^2)
$\bar{t}$: dimensionless time
T: temperature (C)
t: time (s)
$T^h(\mathbf{x})$: trial approximation for temperature
$\bar{T}$: prescribed temperature
v :test (weight) function
Ve: Vernotte number
Δt: time step (s)

*Corresponding author
Email address: i_ahmadi@znu.ac.ir

Greek symbols:
α: thermal diffusivity ($1/s$)
Γ_q: Neumann boundary,
Γ_T: Dirichlet (essential) boundary,
Ω_s^I: local sub-domain around node I
$\partial\Omega_s^I$: boundary of local sub-domain around node I
β: Penalty parameter
$\phi^I(\mathbf{x})$: shape function of the MLS
ρ: mass density (kg/m^3)
η: *integration* parameter
τ_0: thermal relaxation time ($1/s$)

1. Introduction

The classical Fourier's law of heat conduction assumes that the phase lag between the heat flux and temperature gradient is zero. By this assumption, Fourier heat conduction leads to parabolic governing equations which theoretically show infinite propagation speed of thermal signals in the material. The experimental approach by Peshkov [1] in 1944 demonstrated the finite speed of heat propagation. Later, in 1968 experiments in solid helium and in other crystalline solids showed the nature of damped wave of heat conduction [2]. Other researchers in 1995 indicated that the heat flows in the nature of damped wave at very low temperatures [3], and at very short duration [4]. On the other hand, the parabolic heat conduction equation and infinite propagation speed of thermal signals is in contradiction with the theory of relativity and with the known mechanisms of heat conduction.

It is well known that the Fourier's heat conduction equation is an approximate model as far as it describes the heat propagation with infinite speed. However, in most cases, the Fourier's heat conduction equation is in excellent description of heat conduction physics since real propagation speeds of heat signals are very high and the model that assumes infinite speed is often sufficient in accuracy and efficiency.

In order to eliminate the paradox of infinite speed of heat wave and to develop a model for heat conduction with finite speed, Cattaneo [5] and Vernotte [6] independently suggested a modified heat-flux model with thermal relaxation time. In their model, heat flow does not start instantaneously, but raises gradually with a relaxation time τ_0 with respect to the temperature gradient. This non-Fourier heat conduction model conjugated with the equation of energy conservation makes (forms) a hyperbolic system of equations which describes a heat propagation with the finite speed $c=(k/\rho c_p \tau_0)^{1/2}$. The hyperbolic equation for heat conduction also previously had been derived by Maxwell [7] in 1867.

In 1994, Ozisik and Tzou [8] point out that the speed of the thermal wave in solids is in the order of 10^5 m/s and in the gases is in the order of about 10^3 m/s. Mitra et al., [3] and Kaminski [9] performed experiments on heat conduction in the processed meat and dry sand and reported the wave speed about $0.1 mm/s$ which is several orders of magnitude smaller than those reported for other engineering materials. Herwing and Beckert [10] presented an experiment and try to reproduce the results of Mitra et al. [3] and Kaminski [9]. The results of their experiment showed that the reported values in [3] and [9] are doubtful. Roetzel et al., [11] analyzed non-Fourier heat conduction experimentally inside a material with non-homogeneous inner structure and measured thermal diffusivity and relaxation time for this material. In the field of engineering, the non-Fourier heat conduction is used in practical engineering problems [12-14] by different authors.

Analytical and numerical methods have been used for solving the hyperbolic heat conduction equations. Among earlier studies which used analytical strategies, one may refer to [15-23]. Taitel [15] introduced an analytical solution for a thin layer with a step change in the temperature of both sides. Baumeister and Hamil [16] studied the temperature wave in a semi-infinite solid subjected to sudden change in the temperature of the wall by Laplace transforms method. Ozisik and Vick [17] investigated the wave nature of heat propagation in a finite slab with isolated boundaries by analytical solution. Tzou [18, 19] studied the damping and resonance characteristics of thermal waves in periodic heating. Frankel et al., [20] used the flux formulation and gave an analytical solution for a finite slab with the rectangular heat pulse. Gembarovic and Majernik [21] presented an analytical solution for a finite slab with

instantaneous and extended heat pulse. In 1995, Tang and Araki [22] used the Laplace transforms method for the solution of hyperbolic heat conduction in a finite medium subjected to periodic thermal disturbance. In 2000, they used the Green's function and finite integral transform technique to solve a finite medium subjected to a pulse surface heating [23].
Numerical methods are also used for analysis of non-Fourier heat conduction problem with various boundary conditions. Among the numerical methods, the finite difference method [24-32] is extensively used to discrete the governing equation of non-Fourier heat transfer in the space domain. Most of the finite difference schemes are based on the first order hyperbolic constitutive model of Cattaneo [6] and Vernotte [7] which is coupled with the local energy balanced equation and use the McCormack's predictor-corrector method for solving the equations. Some other researchers combined the Cattaneo and Vernotte's model by the local energy balance equation and obtained the second-order hyperbolic equation in terms of temperature, which yields the so-called thermal wave equation, and directly solved the second order wave equation [30-32]. The main problem in the numerical solution of the hyperbolic heat conduction equations is the presence of fictitious numerical oscillations in the results in sharp propagation fronts, which physically is unrealistic [26, 28].
The finite element method [33-37] is also employed for analysis of non-Fourier heat transfer problems. Tamma and Railkar [33] used the finite element method with special shape functions to remove the fictitious numerical oscillations from the results. Manzari and Manzari [34] used a mixed approach to finite element analysis of hyperbolic heat conduction problems. Ai and LiA [35] introduced a discontinuous finite element method for analysis of non-Fourier heat conduction. Wu and Li [36] extended the time discontinuous Galerkin finite element method to the heat wave propagation problem in the medium subjected to different kinds of heat source. Wang and Han [37] used the finite element space discretization for non-Fourier heat conduction and solved the obtained differential equations in time with different time integration methods.
Mishra et al., [38] solved the energy equation of combined radiation and non-Fourier effect by the lattice Boltzmann method (LBM) combined with the finite volume method (FVM).
Vishwakarma et al., [39] in 2011 employed the smoothed particle hydrodynamics method for analysis of the non-Fourier heat transfer in a slab with initial temperature and convection boundary conditions.
The meshless methods are used previously for analysis of the steady-state and transient heat conduction based on the Fourier heat transfer [40-44].
In general, commercial finite element codes are not available for analysis of non-Fourier heat conduction problems. In this study, a meshless formulation is presented for analysis of the non-Fourier heat conduction. In the presented meshless method, the second order wave equation of non-Fourier heat conduction is discretized to the second order ordinary differential equations in time. For solving the obtained equations, a set of new variables is defined and the second order discretized differential equation is written as a first order differential equations. A numerical integration method is used for time integration of the equations. On the other hand, an analytical series solution is obtained for non-Fourier heat conduction in a one-dimensional finite domain for two kinds of boundary conditions. In addition, the predictions of the presented meshless formulation are compared with the predictions of the presented series solution. It is seen that the fictitious numerical oscillations can be suppressed and removed from the numerical results. The numerical results show that the presented meshless method and the time integration scheme could predict temperature wave propagation with a sharp discontinuity in the wave front and without fictitious numerical oscillations.

2. Theoretical modeling

The heterogeneous domain is considered as some homogeneous domain which is bonded together in the interfaces. The continuity conditions in the interfaces couple the governing equations of the domains. So in this study, the governing equation is discretized for the homogeneous equation, and the continuity conditions in the interfaces are enforced to the discretized equations.

2. 1 Governing equations

In order to eliminate the paradox of infinite propagation speed of thermal signals in the Fourier heat conduction, Cattaneo, 1985 and Vernotte, 1958 suggest a modified time-dependent relaxation heat flux model as:

$$\begin{aligned} &\tau_0 \dot{q}_i + q_i = -k T_{,i} \\ &\tau_0 \frac{\partial q_i}{\partial t} + q_i = -k \frac{\partial T}{\partial x_i} \end{aligned} \tag{1}$$

where q_i is the heat flux in the x_i direction, T is the temperature, k is the thermal conductivity and τ_0 is a new parameter which is named thermal relaxation time. In the present study, subscript follows a comma i.e. $T_{,i}$ which shows the partial derivation with respect to x_i and the upper dot on the variable i.e. $\dot{T}$ shows the partial differential with respect to time. The equation of the balance of heat energy in the differential form can be written as:

$$\rho c_p \dot{T} + q_{i,i} = g \tag{2}$$

in which ρ is the mass density and c_p is the specific heat capacity of the material. By elimination of the heat flux from Eqs. (1) and (2), the second order equation of non-Fourier heat conduction can be obtained as:

$$\tau_0 \rho c_p \ddot{T} + \rho c_p \dot{T} = k T_{,jj} + g + \tau_0 \dot{g} \tag{3}$$

in which j is the dummy index. The appropriate Dirichlet and Neumann boundary conditions for Eq. (3) can be considered as:

$$\begin{aligned} &T = \bar{T}, && on \ \Gamma_T \\ &k \frac{\partial T}{\partial n} = -(\bar{q} + \tau_0 \dot{\bar{q}}), && on \ \Gamma_q \end{aligned} \tag{4}$$

In Eq. (4), $\bar{T}$ is the prescribed temperature on Γ_T and $\bar{q}(t)$ is the prescribed heat flux on Γ_q. Equation (3) is in the form of the hyperbolic differential equation and its solution leads to propagation of thermal waves with finite speed as $c=\sqrt{(\alpha/\tau_0)}$ in which $\alpha=k/\rho c_p$ is the thermal diffusivity of the material. From Eq. (3), it is clear that $\tau_0=0$ leads to the parabolic equation of classic Fourier heat diffusion with infinite propagation speed.

In this section, a meshless formulation based on the local weak formulation is presented for discretization of the non-Fourier heat conduction equation in the space domain to second order ordinary differential equations. Then an appropriate method is employed to integrate the discretized equations in the time domain to obtain the propagation of the heat wave in the material.

2.2. Meshless discretization

The generalized local weak form of Eq. (3) in an arbitrary local sub-domain Ω_s^I can be written as:

$$\begin{aligned} &\int_{\Omega_s^I} (\tau_0 \rho c_p \ddot{T} + \rho c_p \dot{T} - k T_{,jj} - (g + \tau_0 \dot{g}) v d\Omega \\ &+ \beta \int_{\Gamma_{sT}^I} (T - \bar{T}) v d\Gamma = 0 \end{aligned} \tag{5}$$

in which the second integral is added to Eq. (5) in order to impose the essential boundary conditions to Γ^I_{sT}. β is a large number which is called penalty parameter and Γ^I_{sT} is a part of the boundary of Ω_s^I which co-inside the Dirichlet boundary conditions and v is the weight function. Now using the divergence theorem the symmetric local weak form of Eq. (5) can be written as:

$$\begin{aligned} &\int_{\Omega_s^I} (\tau_0 \rho c \ddot{T} + \rho c \dot{T} - (g + \tau_0 \dot{g}) v d\Omega + \int_{\Omega_s^I} k T_{,i} v_{,i} d\Omega \\ &- \int_{\partial \Omega_s^I} k T_{,i} n_i v d\Omega + \beta \int_{\Gamma_{sT}^I} (T - \bar{T}) v d\Gamma = 0 \end{aligned} \tag{6}$$

which $\partial\Omega_s^I$ is the boundary of Ω_s^I. By applying the boundary conditions to Eq. (6), it can be written as:

$$\begin{aligned} &\int_{\Omega_s^I} (\tau_0 \rho c \ddot{T} + \rho c \dot{T} - (g + \tau_0 \dot{g})) v d\Omega \\ &+ \int_{\Omega_s^I} k T_{,i} v_{,i} d\Omega + \int_{\Gamma_{sq}^I} (\bar{q} + \tau_0 \dot{\bar{q}}) v d\Omega \\ &- \int_{L_s^I \cup \Gamma_{sT}^I} k T_{,i} n_i v d\Omega + \beta \int_{\Gamma_{sT}^I} (T - \bar{T}) v d\Gamma = 0 \end{aligned} \tag{7}$$

where Γ^I_{sq} is the part of $\partial\Omega_s^I$ over which the natural boundary condition is specified as Eq. (4) and L_s^I is a part of $\partial\Omega_s^I$ which is totally located inside the global domain.

Without losing the generality, the weight function v can be chosen in such a way that it vanishes on L_s^I, so Eq. (7) can be rewritten as:

$$\begin{aligned}&\int_{\Omega_s^I}(\tau_0\rho c\ddot{T}+\rho c\dot{T}-(g+\tau_0\dot{g}))vd\Omega\\&+\int_{\Omega_s^I}kT_{,i}\,v_{,i}d\Omega+\int_{\Gamma_{sq}^I}(\bar{q}+\tau_0\dot{\bar{q}})vd\Omega\\&-\int_{\Gamma_{sT}^I}kT_{,i}\,n_i vd\Omega+\beta\int_{\Gamma_{sT}^I}(T-\bar{T})\,vd\Gamma=0\end{aligned}\tag{8}$$

As noted before, Ω_s^I is local sub-domain around node I in the domain and the nodes are scattered randomly in the global domain Ω. The moving least square (MLS) approximation method is used for discretization of Eq. (8). Using the MLS method the trial function for the field variable can be written as:

$$T^h(\mathbf{x})=\sum_{J=1}^{N}\phi^J(\mathbf{x})\hat{T}^J\qquad \mathbf{x}\in\mathbf{\Omega_x}\tag{9}$$

where $\phi^I(\mathbf{x})$ is usually called the shape function of the MLS approximation corresponding to node I and $\hat{T}^I$ is called the fictitious nodal values in node I. The details of construction of the shape function by MLS method can be found in [44].

Now for discretization of Eq. (8), the MLS approximation is substituted from Eq. (9) into Eq. (8) as:

$$\begin{aligned}&\int_{\Omega_s^I}(\tau_0\rho c\phi^J\,\ddot{\hat{T}}^J+\rho c\phi^J\,\dot{\hat{T}}^J-(g+\tau_0\dot{g}))vd\Omega\\&+\int_{\Omega_s^I}k\phi_{,i}^J\,v_{,i}\hat{T}^J\;d\Omega+\int_{\Gamma_{sq}^I}(\bar{q}+\tau_0\dot{\bar{q}})vd\Omega\\&-\int_{\Gamma_{sT}^I}k\phi_{,i}^J\,n_i\hat{T}^J vd\Omega+\beta\int_{\Gamma_{sT}^I}(\phi^J\,\hat{T}^J-\bar{T})\,vd\Gamma=0\end{aligned}\tag{10}$$

Equation (10) is the discretized governing equations of non-Fourier heat transfer. It can be written in the standard form as

$$D_{IJ}\ddot{\hat{T}}^J+C_{IJ}\dot{\hat{T}}^J+K_{IJ}\hat{T}^J=f_I\tag{11}$$

in which the matrices are defined as:

$$\begin{aligned}D_{IJ}&=\int_{\Omega_s^I}\tau_0\rho c\phi^J vd\Omega\\C_{IJ}&=\int_{\Omega_s^I}\rho c\phi^J vd\Omega\\K_{IJ}&=\int_{\Omega_s^I}k\,\phi_{,i}^J v_{,i}d\Omega-\int_{\Gamma_{su}^I}k\,\phi_{,i}^J n_i vd\Gamma+\beta\int_{\Gamma_{su}^I}\phi^J vd\Gamma\\f_I&=\int_{\Omega_s^I}(g+\tau_0\dot{g})v\,d\Omega-\int_{\Gamma_{sq}^I}(\bar{q}+\tau_0\dot{\bar{q}})vd\Gamma+\beta\int_{\Gamma_{su}^I}\bar{T}vd\Gamma\end{aligned}\tag{12}$$

3. Numerical time integration

After spatial discretization of the governing equations, the obtained ordinary differential equation must be integrated into the time domain. For time integration, the second order differential equations are converted into a set of the first order differential equation. The new set of variables is defined as:

$$\{x\}=\{\hat{T}^J,\dot{\hat{T}}^J\}^T\tag{13}$$

Using the new set of variables in Eq. (13), the second order equation in Eq. (11) can be written as:

$$[A]\{\dot{x}\}+[B]\{x\}=\{F\}\tag{14}$$

in which

$$[A]=\begin{bmatrix}[I]&[0]\\[0]&M_{IJ}\end{bmatrix},\;[B]=\begin{bmatrix}[0]&-[I]\\K_{IJ}&C_{IJ}\end{bmatrix},\;\{F\}=\begin{Bmatrix}\{0\}\\f_I\end{Bmatrix}\tag{15}$$

For time integration of Eq. (14), an appropriate finite difference method is used. Using the backward difference approximation, the governing Eq. (14) at the time t=t_m can be written as:

$$[A](\frac{\{x\}_m-\{x\}_{m-1}}{\Delta t})+[B]\{x\}_m=\{F\}_m\tag{16}$$

By replacement of m with m+1, $\{x\}_{m+1}$ can be obtained from Eq. (16) as:

$$\{x\}_{m+1}=([A]+\Delta t[B])^{-1}([A]\{x\}_m+\Delta t\{F\}_{m+1})\tag{17}$$

Using the forward difference approximation, Eq. (14) at the time t=t_m can be written as:

$$[A](\frac{\{x\}_{m+1}-\{x\}_m}{\Delta t})+[B]\{x\}_m=\{F\}_m \tag{18}$$

$\{x\}_{m+1}$ can be obtained by solution of Eq. (18) as:

$$\{x\}_{m+1}=(I+\Delta t[A]^{-1}[B])\{x\}_m+\Delta t[A]^{-1}\{F\}_m \tag{19}$$

In general, solution of Eq. (14) can be obtained by combination of the forward difference and backward difference method as:

$$\begin{aligned}&(\frac{[A]}{\Delta t}+\eta[B])\{x\}_{m+1}=\\&(\frac{[A]}{\Delta t}-(1-\eta)[B])\{x\}_m+(1-\eta)\{F_m\}+\eta\{F_{m+1}\}\end{aligned} \tag{20}$$

where $0\leq\eta\leq1$ is a real parameter. For η=0, Eq. (20) is known as the forward difference method, for η=1 it is known as the backward difference method, for η=0.5 it is known as Crank-Nicolson method and for η=2/3 it is known as Galerkin method. The effect of η parameter on the numerical results of time integration Eq. (20) is investigated in the present study.

The solution algorithm of equations based on the meshless method is as follows.

a) Nodes are scattered in the solution domain and MLS is used to make the interpolation functions.
b) The integrations over the subdomains in Eq. (12) are done based on the Gussian integration method for all of the subdomains around the nodes and the discretized equations are obtained.
c) The numerical integration method in Eq. (20) is used for time integration of the discretized equations and the time history of the temperature is obtained.

4. Analytical solution for 1D domain

For a 1D finite domain which one boundary is subjected to a temperature shock and the other boundary is kept isolated or is kept at constant temperature, the analytical series solution for the non-Fourier heat transfer is obtained. The results of this analytical series solution are used to verify the accuracy and efficiency of the presented meshless formulation and the numerical integration method.

Consider a 1D finite isotropic domain with the length L and the spatial coordinate x, $0\leq x\leq L$ which its thermal diffusivity is α. For generality of solution and numerical results, the following dimensionless parameters are defined as:

$$\bar{x}=\frac{x}{L},\quad \bar{t}=Fo=\frac{\alpha t}{L^2},\quad Ve^2=\frac{\alpha\tau_0}{L^2} \tag{21}$$

in which $\bar{x}$ is the dimensionless spatial co-ordinate, $\bar{t}=Fo$ is a dimensionless variable for time and is called Fourier number and Ve is the Vernotte number. By employing the above dimensionless parameters, the second order equation of non-Fourier heat transfer in Eq. (3) for 1D domain can be written as:

$$V_e^{\,2}\frac{\partial^2 T}{\partial \bar{t}^2}+\frac{\partial T}{\partial \bar{t}}=\frac{\partial^2 T}{\partial \bar{x}^2}+\frac{L^2}{k}(g+\tau_0\dot{g}) \tag{22}$$

and in the absence of the heat source, the above equation could be written as:

$$V_e^{\,2}\frac{\partial^2 T}{\partial \bar{t}^2}+\frac{\partial T}{\partial \bar{t}}=\frac{\partial^2 T}{\partial \bar{x}^2} \tag{23}$$

In the next section, a series solution is obtained for Eq. (23) for two types of boundary conditions (B.Cs) at x=L. The initial value for temperature and temperature rate are zero and the B.C in the right side is different.

B.C type 1- The left side of the domain is suddenly subjected to a temperature shock (change) as T_1 at $t=0^+$ and the right side is kept isolated and the initial conditions are zero.

B.C type 2-The left side of the domain is suddenly subjected to a temperature shock (change) as T_1 at $t=0^+$ and the right side is kept at fixed temperature T_2=0 and the initial conditions are zero.

4.1. Isolated boundary at right side

Consider the domain with zero initial temperature $T(x, t=0)=0$ and zero initial rate of temperature change $\dot{T}$ (x, t=0)=0. At $t=0^+$, the left side (x=0) is suddenly subjected to constant temperature jump as T_1 and the right side (x=L) is kept isolated. The series solution of (23) for these boundary and initial conditions can be obtained as:

$$T(\bar{x},\bar{t})=$$
$$T_1(1-\sum_{n=1,3,...}^{\infty}\frac{4}{n\pi}[A_n\exp(\lambda_{1n}\bar{t})+B_n\exp(\lambda_{2n}\bar{t})]\sin(\frac{n\pi\bar{x}}{2})) \tag{24}$$

in which λ_{1n} and λ_{2n} are the roots of the following equation

$$(Ve)^2\lambda_n^{\ 2}+\lambda_n+(\frac{n\pi}{2})^2=0 \tag{25}$$

and A_n and B_n must be obtained from the initial conditions. For zero initial conditions, the coefficients A_n and B_n can be obtained as:

$$A_n=\frac{\lambda_{2n}}{\lambda_{2n}-\lambda_{1n}},\quad B_n=\frac{-\lambda_{1n}}{\lambda_{2n}-\lambda_{1n}} \tag{26}$$

The series solution of this problem for the classical Fourier heat conduction theory can be obtained as:

$$T(\bar{x},\bar{t})=T_1(1-\sum_{n=1,3,...}^{\infty}\frac{4}{n\pi}\exp(\lambda_n\bar{t})\sin(\frac{n\pi\bar{x}}{2})) \tag{27}$$

in which λ_n=-$(n\pi/2)^2$.

4.2. Constant temperature at right side

A sudden fixed temperature jump at the left side (x=0) as $T(0,t^+)=T_1$ is considered and the right side is kept at constant temperature T_2=0, and the initial conditions are zero. For these boundary conditions, the solution of Eq. (21) can be obtained as

$$T(\bar{x},\bar{t})=T_1(1-x/L)-T_1\sum_{n=1}^{\infty}\frac{2}{n\pi}[A_n\exp(\lambda_{1n}\bar{t}) + B_n\exp(\lambda_{2n}\bar{t})]\sin((n\pi x)/L) \tag{28}$$

where λ_{1n} and λ_{2n} are the roots of the characteristic equation as:

$$(Ve)^2\lambda_n^{\ 2}+\lambda_n+(n\pi)^2=0 \tag{29}$$

For zero initial conditions, A_n and B_n can be obtained the same as Eq. (26). The series solution of the same problem for the classical Fourier heat conduction theory can be obtained as:

$$T(\bar{x},\bar{t})=$$
$$T_1(1-x/L)-T_1\sum_{n=1}^{\infty}\frac{2}{n\pi}\exp(\lambda_{1n}\bar{t})\sin(n\pi x/L) \tag{30}$$

in which λ_n=-$(n\pi)^2$. The series solutions which are obtained in these sections are employed for verification of the results of presented meshless method.

5. Numerical results and discussions

Due to the hyperbolic nature of the non-Fourier heat transfer, the propagating of the temperature in the domain has the wavy form. In the numerical solutions, in order to obtain reasonable accuracy in the solution of the non-Fourier equations, the nodes must be dense enough and the chosen time step Δt for numerical integration must be small enough for obtaining the sharp discontinuity in the wave front. So, the solutions of 2D and 3D problems lead to relatively heavy computational cost. In this study, in order to avoid the excessive computational time, and to examine the efficiency and accuracy of the method, one-dimensional heat transfer is studied in the numerical results.

A 1D finite isotropic domain with the spatial coordinate x and the length L is considered in which the physical properties of the domain are k, c_p, ρ and τ_0 and so the thermal diffusivity of the domain can be obtained as $\alpha=k/\rho c_p$. According to the non-Fourier heat transfer, the speed of the temperature waves can be obtained as $c=\sqrt{(\alpha/\tau_0)}$. The typical value for the thermal diffusivity is about $\alpha\sim10^{-4}$ m^2/s and for relaxation time is about $\tau_0\sim10^{-12}$ s and so the speed of the temperature wave can be obtained as $c=\sqrt{(\alpha/\tau_0)}\sim10^4$ m/s. Tzou and Chen, 1998 [45] estimated time constants for non-Fourier effect are of the order of micro-to picoseconds.

Now the new parameter c^* is defined as $c^*=1/Ve$ and from Eq. (21) it can be concluded that:

$$\bar{t}\,c^*=ct/L=\bar{x} \tag{31}$$

So it is clear that c^* is the dimensionless speed of the temperature waves. Now τ^* is defined the dimensionless time in which the temperature waves (disturbances) travel across the domain from the left side ($\bar{x}$=0) to the right side ($\bar{x}$=1). According to the definition of the dimensionless speed c^*, it is clear that $\tau^*=1/c^*=Ve$. So any disturbance at the left side will be sensed at the right side at $\bar{t}=\tau^*=Ve$.

5.1. Parameters study

The effect of the parameters such as η, $\Delta\bar{t}$ and the number of nodes on the predictions of the meshless method is studied in this section for two kinds of boundary conditions. The domain with the initial and boundary conditions of type 1 is considered i.e. the left side is subjected to sudden temperature jump as $T_l=1$ at $\bar{t}=0^+$ and the right side is kept isolated and the initial conditions are zero. The series solution of this problem is obtained in Eq. (24).

At first, the effects of η parameter (see Eq. (20)) on the numerical results of the time integration are studied. In the space discretization by the meshless method, 401 nodes are scattered in the domain $0 \le \bar{x} \le 1$. In the time integration method which is introduced in Eq. (20), the parameter η will affect the results of the numerical integration. As noticed before, the η parameter, ($0\le\eta\le1$), can be chosen in the time integration and for $\eta=1$, $\eta=0.5$ and $\eta=0$ the integration method is known as backward difference method, Crank-Nicolson method, and forward difference method, respectively. For $\eta=2/3$ it is known as Galerkin method. In the numerical analysis in this study, it is seen that for $\eta<0.5$ the time integration is unstable and does not converged. For Ve=1, the results of the time integration for different values of $\eta\ge0.50$ and the chosen time step as $\Delta\bar{t}=0.001\tau^*$ are seen in Fig. 1. This figure shows the distribution of the temperature in the domain at $\bar{t}=0.1\tau^*$, $\bar{t}=0.5\tau^*$, $\bar{t}=0.9\tau^*$ and $\bar{t}=1.4\tau^*$. As seen in Fig. 1, for $\bar{t}<\tau^*$ the wave is traveling from the left to the right of the domain and for $\bar{t}>\tau^*$ the wave is reflected and is traveling from the right to the left. The moving direction of the wave is shown in the figure. In Fig. 1, the best sharpness in the discontinuity in the wave front is seen for $\eta=0.50$. Also for $\eta=0.50$ the fictitious numerical oscillations are seen near the wave front. As seen in Fig. 1, for $\eta\ge0.55$, the fictitious oscillations are suppressed from the results, and the sharpness of the discontinuity in the wave front is decreased by increasing η. The best value for η is the value that suppresses the fictitious oscillation and gives the sharpness in the wave front. So the best value of η must be near to 0.5. The analysis shows that $\eta=0.55$ is a good value for η because for $\eta=0.55$ no fictitious oscillations are seen in the results and the sharpness of the wave front is good. In the next results, $\eta=0.55$ is used in the numerical integration.

The effects of the dimensionless time step $\Delta\bar{t}$ on the numerical results of the time integration are investigated in Fig. 2. The results of numerical integration for $\Delta\bar{t}=0.005\tau^*$, $\Delta\bar{t}=0.002\tau^*$, $\Delta\bar{t}=0.001\tau^*$, $\Delta\bar{t}=0.0005\tau^*$ with $\eta=0.55$ are shown in Fig. 2. In Fig. 2, 401 nodes are used for space discretization of the domain. As it can be seen in this figure, for $\Delta\bar{t}=0.005\tau^*$ and $\Delta\bar{t}=0.002\tau^*$, fictitious numerical oscillations are seen in the results. The results show that by decreasing $\Delta\bar{t}$, the oscillation is suppressed and the sharpness of the discontinuity is increased. In the next results $\Delta\bar{t}=0.001\tau^*$ is used as the time step in the numerical integration.

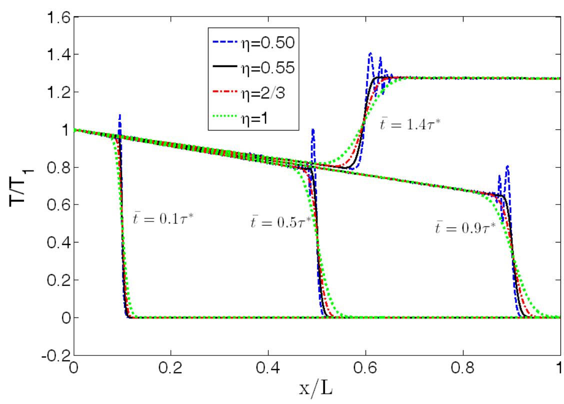

Fig. 1. The results of numerical integration for various value for η, (Ve=1)

The effect of the number of nodes in meshless discretization on the numerical results is shown in Fig. 3. The results are shown for 101, 201, 401 and 801 nodes in the domain. In the results of Fig. 3, the dimensionless time step $\Delta\bar{t}$=0.001τ^* is used for numerical integration of the equations. It is seen that some numerical oscillations are seen for 101 and 201 nodes. There are no oscillations for 401 and 801 nodes and increase of nodes from 401 to 801 increased the computational cost but the predictions of 401 nodes are very close to the predictions of 801 nodes. So in the next results, 401 nodes are used in the meshless space discretization of the equations.

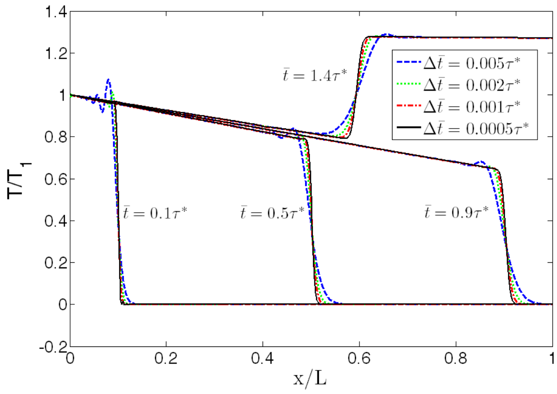

Fig. 2. The effect of dimensionless time step $\Delta\bar{t}$ on the results of numerical integration.

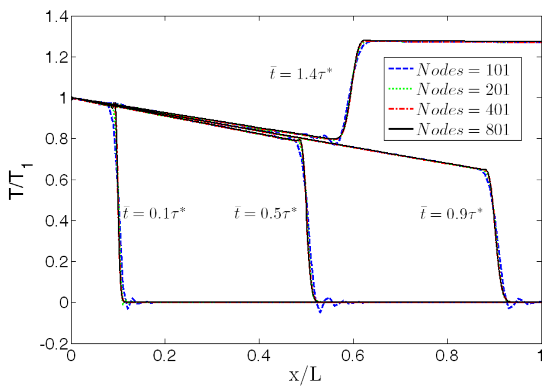

Fig. 3. Effect of the number of nodes on the predictions of the meshless method.

5. 2. Validation of the results

For validation of the accuracy of the predictions of the meshless method and the integration method, the predictions of the presented meshless method are compared with the predictions of the obtained series solution. In the results of the meshless method, 401 nodes are used for spatial discretization, the dimensionless time step is chosen as $\Delta\bar{t}$=0.001τ^* and η=0.55.

5. 2. 1 Boundary conditions type 1

The right side of the domain is isolated and the left side is subjected to constant temperature shock as T_1=1 at t=0^+ (B.C type 1). The series solution for this problem is obtained in Eq. (24). The comparison of the prediction of the meshless method and analytical solution for Ve=1 are shown in Fig. 4. As seen in Fig. 4, the temperature shock in the left side travels to the right with the speed c^*=1/τ^*=Ve. In $\bar{t}$<τ^* the front of the wave does not reach to the isolated boundary at x=L, but for $\bar{t}$>τ^* the wave is reflected from the right boundary. The dashed lines show the predictions of the meshless method and the solid lines show the predictions of the analytical series solution. It is seen that there is good agreement between the predictions of the meshless method and series solution, except for the wave front which is completely sharp in the prediction of the analytical method. As seen in Fig. 2 the sharpness of the wave front in numerical solution increases by decreasing of the $\Delta\bar{t}$.

For analysis of the effects of Ve number on the numerical results, the predictions of the present meshless method and series solution for Ve=4 are shown in Fig. 5. By comparing Fig. 4 with Fig. 5 it is evident that for Ve=1 the height of the wave front is decreased as the wave travel in the domain and when the wave reaches to x=L the wave front height is about 0.63 and the wave is reflected by the height about 1.25. For Ve=4 the decreasing rate of the wave height is smaller and the wave height at x=L is about 0.89 and it is reflected by the height about 1.77. It is concluded that by increasing the Ve, the effect of damping decreases and the temperature wave will be damped to the final steady state temperature very slowly.

The propagation of the temperature in the domain with Ve=0.1 is shown in Fig. 6. The predictions of non-Fourier and Fourier heat conduction theories will be close for a small Ve number. This figure contains the prediction of a series solution and meshless solution for both hyperbolic (non-

Fourier) and parabolic (Fourier) heat conduction equations. The first conclusion is that the predictions of the numerical solution are in close agreement with the predictions of analytical series solution for both Fourier and non-Fourier heat conduction. A look at Fig. 6 make it clear that for *Ve*=0.1, in the non-Fourier theory the wave front is damped very quickly. Fig. 6 also shows the predictions of the parabolic heat transfer equations i.e. *Ve*=0. It can be seen that the form of the temperature propagation by hyperbolic equations with *Ve*=0.1 is very close to temperature diffusion by parabolic equation i.e. *Ve*=0. For hyperbolic equation with *Ve*=0.1 the dimensionless speed of temperature wave is $c^*=10$ and as known in the parabolic equation the temperature diffuse with infinity speed, so as seen in Fig. 6 for $\bar{t}=1.4\tau^*$ the prediction of the parabolic equation is over than the prediction of the hyperbolic equation.

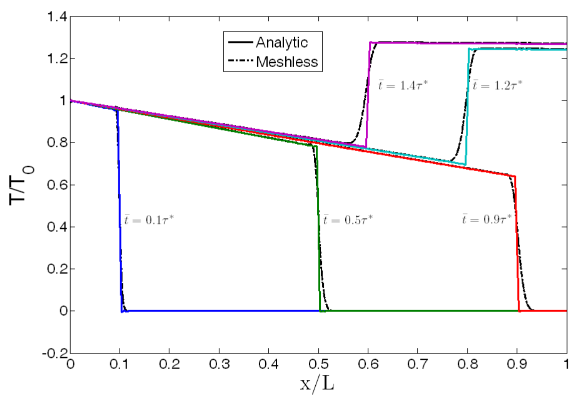

Fig. 4. Comparison the results of meshless method with analytical solution (Ve=1, $\Delta\bar{t}=0.001\tau^*$).

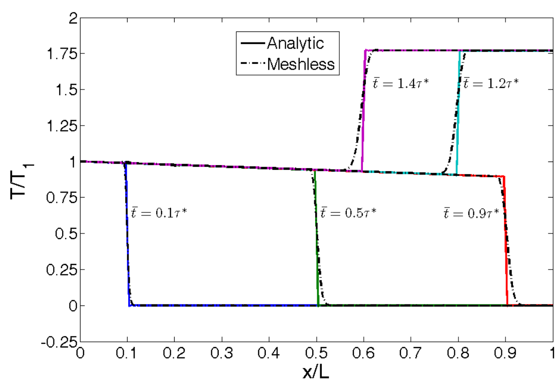

Fig. 5. Propagation of temperature shock in the domain for *Ve*=4, meshless method and analytical method.

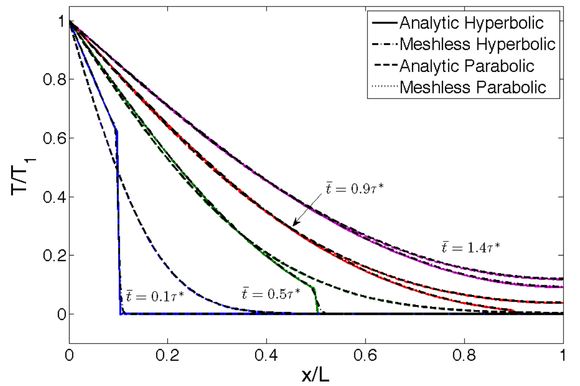

Fig. 6. Comparison the results of temperature propagation with *Ve*=0.1 and temperature diffusion.

5. 2. 2 Boundary conditions type 2

To study the effect of the boundary conditions of the right side on the propagation of the wave, in this problem the boundary temperature at the right side of domain at $x=L$ is kept constant at the initial temperature $T_2=0$, and same as the previous problem, the initial conditions are zero and the left boundary at $x=0$ is suddenly subjected to a temperature shock as $T_1=1$ at $\bar{t}=0^+$. The series solution of the problem is introduced in section 4-2. Same as before, for numerical solution 401 nodes are used in meshless discretization and $\Delta\bar{t}=0.001\tau^*$. The propagation of temperature in the domain for *Ve*=1 is shown in Fig. 7.

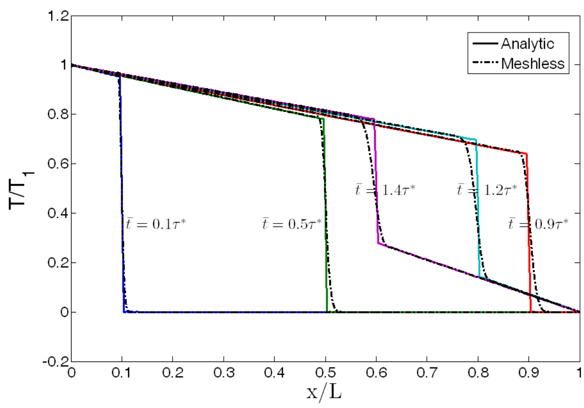

Fig. 7. Propagation of temperature shock in the domain with fixed temperature at $x=L$ (Ve=1).

As it can be seen the temperature disturbance in the left side travels to the right side, so before $\bar{t}=\tau^*$ the wave front does not sense the boundary condition at $x=L$. So as it can be seen in Figs. 7 and 4, for both isolated boundary and fixed temperature boundary at $x=L$, for $\bar{t}<\tau^*$, the temperature distribution is completely the same. At $\bar{t}=\tau^*$ the wave front senses the right side boundary and for $\bar{t}>\tau^*$ the wave is affected by the boundary conditions of the right side. As seen in Figs. 7 and 4, for $\bar{t}>\tau^*$ the wave reflection is different for the isolated boundary and fixed temperature boundary. Also, in order to compare the numerical results of the present meshless method with the available results in the literature, the predictions of the present method are compared with the predictions of the analytical method which is presented in [46]. The domain which is isolated both at $x=0$ and $x=L$ is considered. The initial temperature distribution in the domain is chosen as $T=2T_0x/L$ for $0<x\leq L/2$, and $T=2T_0(1-x/L)$ for $L/2<x<L$. The time history of the temperature in the left edge of the domain ($x=0$) is shown in Fig. 8. The prediction of the present meshless method and analytical method [46] are shown in this figure. Good agreement is seen between the prediction of the meshless method and analytical method [46] in prediction the time history of temperature. From Figs. 4 to 8, it is seen that the predictions of the present meshless method are in good agreement with the predictions of the analytical method. Therefore, it can be concluded that the present method has good accuracy in the solution of the non-Fourier heat transfer problems.

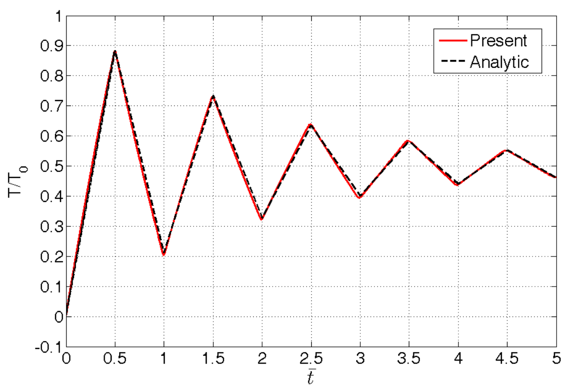

Fig. 8. Time history of the left edge ($x=0$) of the domain ($Ve=1$), prediction of meshless method (solid line) and analytic method [46] (dashed line).

5. 3. Time history of temperature

For a slab with a zero initial temperature which is subjected to a temperature shock at the left side as $T_1=1$, the time history of the temperature of point A which is located at $x=L/2$ is depicted in Fig. 9. This figure contains the prediction of both theories; non-Fourier heat conduction with $Ve=1$ (temperature propagation with hyperbolic equation) and Fourier heat conduction (temperature diffusion with parabolic equation). The time history of temperature is studied for both fixed temperature at the right side ($T_2=0$) and also for the isolated boundary at the right side. As presented in the Fig. 9, in the non-Fourier theory (hyperbolic equation) the wave propagates from the left side to the right and at $\bar{t}=0.5\tau^*$ wave passes from point A which is located at $x=L/2$. At $\bar{t}=\tau^*$ the wave reaches to the right side of the domain. In non-Fourier theory as it can be seen in Fig. 9 before $\bar{t}/\tau^*=0.5$, the point at $x=L/2$ does not sense the temperature shock. At $\bar{t}/\tau^*=1$ the wave riches the right boundary and is reflected and at $\bar{t}/\tau^*=1.5$, the point A senses the effect of the reflection from the right boundary. So as seen in Fig. 8, for $\bar{t}/\tau^*<1.5$ the temperature of point A which is located at $x=L/2$ is the same for the both kinds of B.C at the right side of the domain. The effect of the right boundary on the temperature of point A is seen for $\bar{t}/\tau^*>1.5$. The wave is reflected from the boundaries and the effect of these reflections is sensed at the point A at $\bar{t}/\tau^*=1.5$, 2.5, 3.5, 4.5, 5.5, … . The height of wave front decreases by each reflection and the temperature tends to steady state value.

The prediction for the temperature of point A by the Fourier heat conduction is also depicted in Fig. 9. It can be seen that in the prediction of the Fourier equation, the temperature shock on the left side is immediately sensed at the point A. For fixed boundary temperature $T_2=0$ at the right side, the temperature of point A increased and riches its steady state value $T=0.5T_1$ at about $\bar{t}=0.5\tau^*$. For isolated right side, the temperature is increased to T_1 and riches its steady state value at about $\bar{t}=2\tau^*$.

The effect of the Ve number on the time history of the propagation of the temperature on the domain is shown in Fig. 10. It also shows the time history of the temperature on point $x=L/2$ for the various Ve number. In Fig. 10, it is seen that by decreasing of the Ve number the prediction of the non-Fourier and Fourier heat conduction theories will be very close. It can be seen that the speed of the propagation of the wave increases by decreasing of the Ve number and the height of the reflection of the waves is decreased by decreasing the Ve number. For Ve=0.1 except at $\bar{t}\leq 0.1\tau^*$ the prediction of non-Fourier and Fourier heat conduction is in very close agreement.

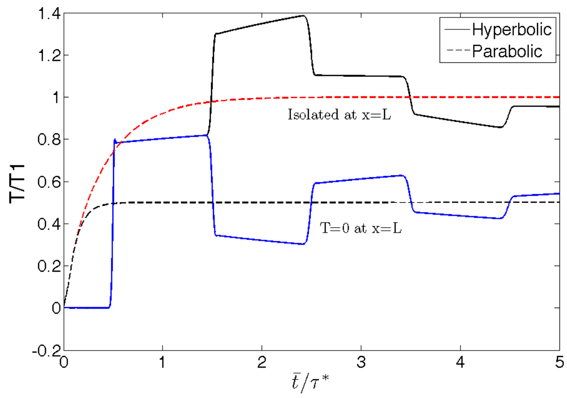

Fig. 9. Time history of temperature at point $x=L/2$, Fourier and non-Fourier theory.

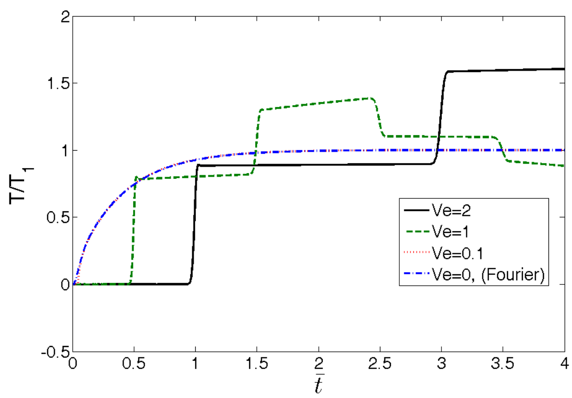

Fig. 10. The effect of Ve number on the time history of the temperature at $x=L/2$.

5. 4. Response to initial conditions

In this section, the propagation of temperature in the slab which is subjected to initial unsteady state temperature distribution is investigated. The slab is subjected to an initial temperature at t=0 as $T=T_0x/L$ for $x\leq L/2$ and $T=T_0(1-x/L)$ for $x>L/2$. First, it is considered that the temperature of boundaries is kept constant at $T_1=T_2=0$.

Figure 11 shows the time history of the distribution of temperature in the slab for $T_1=T_2=0$ for Ve=1. It is seen that the initial temperature distribution oscillated such as a vibrating string with damping and at $\bar{t}=\tau^*$ the distribution is reversed but the height is decreased. At $\bar{t}=2\tau^*$ the temperature at $x=L/2$ is decreased from $T_0/2$ to about $0.18T_0$.

The distribution of the temperature in the slab with the same initial conditions but with an isolated boundary at the left and right sides are presented in Fig. 12. The steady state temperature for this case is $T=T_0/4$ and so as seen the initial temperature oscillates about $T=T_0/4$. The form of variation of the temperature in the domain is clearly shown in the figures.

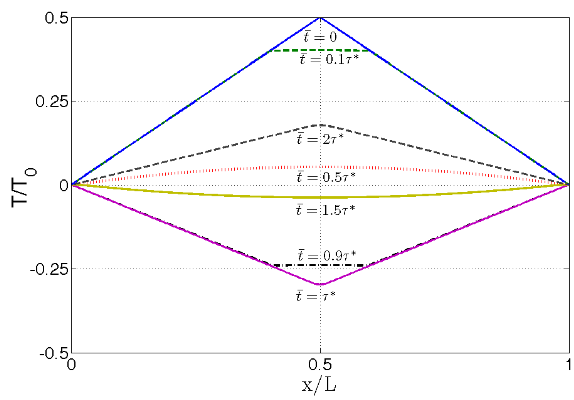

Fig. 11. Time history of the temperature distribution at the slab for fixed boundary temperatures $T_1=T_2=0$.

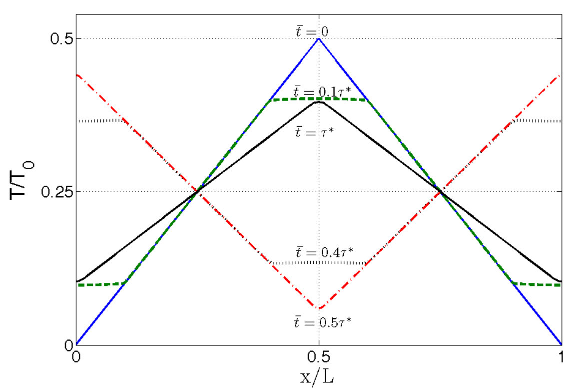

Fig. 12. Time history of the temperature distribution at the slab for isolated boundaries.

6. Conclusions

In this study, a truly meshless formulation is derived for the analysis of heat conduction based on the non-Fourier heat conduction theorem. The hyperbolic equation of non-Fourier heat conduction is discretized in the space domain to a system of ordinary differential equations in the time domain. The penalty parameter method is used for enforcement of the essential boundary conditions to the equations. A kind of finite difference method is used for time integration of the equations so that the fictitious isolations in the numerical results are suppressed. The presented formulation is general for 3D heat transfer. An analytical series solution is derived for the hyperbolic equation of non-Fourier heat conduction in a 1D domain for two types of boundary conditions. In the numerical results, the non-Fourier heat conduction in a slab is studied. A parametric study is done on the effect of the time integration parameter, dimensionless time step in the numerical integration and on the number of nodes in the meshless discretization. The series solution is employed to examine the accuracy of the predictions of the numerical method. It is shown that there is good agreement between the predictions of the numerical method and series solutions. It is concluded that the presented meshless method is efficient and accurate in the solution of non-Fourier heat conduction and it can be used for analysis of non-Fourier heat transfer in solid structures.

References

[1] V. Peshkov, “Second sound in helium II”, *J. Phys. USSR*, Vol. 8, No.1, pp. 381-388, (1944).

[2] C. C. Ackerman, and R. A. Guyer, “Temperature pulse in dielectric solids”, *Ann. Phys.*, Vol. 50, No. 1, pp. 128-185, (1968).

[3] K. Mitra, S. Kumar, A. Vedaraz, and M. K. Moallemi, “Experimental evidence of hyperbolic heat conduction in processed meat”, *ASME J. Heat Transfer*, Vol. 117, No. 3, pp. 568-573,(1995).

[4] Y. S. Xu and Z. Y. Guo, “Heat wave phenomena in IC chips”, *Int J Heat Mass Transfer*, Vol. 38, No. 15, pp. 2919-2922, (1995).

[5] C. Cattaneo, “Sur une forme de l’equation de la chaleur eliminant le paradoxe d’ine propagation instantanee”, *C. R. Acad. Sci.*, Vol. 247, pp. 431-433, (1958).

[6] P. Vernotte, “Les paradoxes de la theorie continue de l’equation de la chaleur”, *C. R. Acad. Sci.*, Vol. 46, No. 22, pp. 3154-3155, (1958).

[7] J. C. Maxwell, “On the dynamical theory of gases”, *Philos. Trans. Royal Soc. London*, Vol. 157, No. 1, pp. 49-88, (1867).

[8] M. N. Ozisik, D. Y. Tzou, “On the wave theory in heat conduction”, *ASME J. Heat Transfer*, Vol. 116, No. 3, pp. 526-535, (1994).

[9] W. Kaminski, “Hyperbolic heat conduction equation for materials with a nonhomogenous inner structure”, *ASME J. Heat Transfer*, Vol. 112, No. 3, pp. 555-560, (1990).

[10] H. Herving, and K. Beckert, “Experimental evidence about the controversy concerning Fourier and non-Fourier heat conduction in materials with a nonhomogeneous inner structure”, *Heat and mass Transfer*, Vol. 36, No. 5, pp. 387-392, (2000).

[11] W. Roetzel, N. Putra and S. K. Das, “Experiment and analysis of non-fourier conduction in materials with non-homogeneous inner structure”, *Int. J. therm. Sci.*, Vol. 42, No. 3, pp. 541-552, (2003).

[12] E. Ruckenstein, and C. A. Petty, “On the aging of supported metal catalyst due to hot spots”, *Chemical Engineering Science*, Vol. 27, No. 5, pp. 937-946, (1972).

[13] R. Ocone, and G. Astarita, “Continuous and discontinuous models for transport phenomena in polymers”, *AIChE Journal*, Vol. 33, No. 3, pp. 423-435, (1987).

[14] A. M. Mullis, “Rapid solidification in the framework of hyperbolic conduction model”, *Int. J. Heat Mass Transfer*, Vol. 40, No. 17, pp. 4085-4097, (1997).

[15] V. Taitel, “On the parabolic, hyperbolic and discrete formulation of the heat conduction equation”, *Int. J. Heat Mass*

Transfer, Vol. 15, No. 2, pp. 369-371, (1972).

[16] K. J. Baumeister, and T. D. Hamill, "Hyperbolic Heat-Conduction Equation—A Solution for the Semi-Infinite Body Problem", *ASME J. Heat Transfer*, Vol. 91, No. 4, pp. 543-548, (1969).

[17] M. N. Ozisik, and B. Vick, "Propagation and reflection of thermal waves in a finite medium", *Int. J. Heat Mass Transfer,* Vol. 27, No. 10, pp. 1845-1854, (1984).

[18] D. Y. Tzou, "Thermal Resonance Under Frequency Excitations", *ASME J. Heat Transfer*, Vol. 114, No. 2, pp. 310-316, (1992)

[19] D. Y. Tzou, "Damping and Resonance Characteristics of Thermal Waves", *ASME J. Appl. Mech*., Vol. 59, No. 4, pp. 862-867, (1992).

[20] J. I. Frankel, B. Vick and M. N. Ozisik, "Flux formulation of hyperbolic heat conduction", *J. Appl. Phys.*, Vol. 58, No, 1, pp. 3340-3345, (1985).

[21] J. Gembarovic and V. Majernik "Non-Fourier propagation of heat pulse in finite medium", *Int. J. Heat Mass Transfer*, Vol. 31, pp. 1073-1081, (1988).

[22] Tang, D.W. and Araki N., "Non-Fourier heat conduction in a finite medium under periodic surface thermal disturbance", *Int. J Heat Mass Transfer*. Vol. 39, No. 8, pp. 1585-1590, (1996).

[23] D. W. Tang, and N. Araki, "Non-Fourier Heat Conduction Behavior in Finite Mediums under Pulse Surface Heating", *Materials Sci. and Eng*., Vol. 292, No. 2, pp. 173-178, (2000).

[24] G. F. Carey, and M. Tsai, "Hyperbolic heat transfer with reflection", *Numerical Heat Transfer Part A*, Vol. 5, No. 3, pp. 309-327, (1982).

[25] D. E. Glass, M. N. Ozisik, D. S. McRae, and B. Vick, "The numerical solution of hyperbolic heat conduction", *Numerical Heat Transfer*, Vol. 8, No. 4, pp. 497-504, (1985).

[26] D. E. Glass, M. N. Ozisik, D. S. McRae, B. Vick, "On the numerical solution of hyperbolic heat conduction", *Numerical Heat Transfer*, Vol.8, No. 4, pp. 497-504, (1985).

[27] D. E. Glass, and M. N. Ozisik, "Non-Fourier Effects on Transient Temperature Resulting from Periodic On-Off Heat Flux", *Int. J. Heat Mass. Transfer*, Vol. 30, No. 8 , pp. 1623-1631, (1987).

[28] H. Q. Yang, "Characteristics-based, high-order accurate and nonoscillatory numerical method for hyperbolic heat conduction", *Numerical Heat Transfer, Part B: Fundamentals*, Vol. 18, No. 2, pp. 221-241, (1990).

[29] B. Pulvirenti, A. Barletta, and E. Zanchini "Finite-Difference Solution of Hyperbolic Heat Conduction with Temperature-Dependent Properties", *Numerical Heat Transfer A*, Vol. 34, No. 2 , pp. 169-183, (1998).

[30] A. Kar, C. L. Chan, and J. Mazumder, "Comparative studies on nonlinear hyperbolic and parabolic heat conduction for various boundary conditions: analytic and numerical solutions", *ASME J. Heat Transfer*, Vol. 114, No. 1, pp. 14-20, (1992).

[31] S. H. Pulko, A. J. Wilkinson, and A. Saidane, "TLM representation of the hyperbolic heat conduction equations", *International Journal of Numerical Modelling: Electronic Networks, Devices and Fields*, Vol. 15, No. 3, pp. 303-315, (2002).

[32] A. L. Koay, S. H. Pulko, and A. J. Wilkinson, "Reverse time TLM modeling of thermal problems described by the hyperbolic heat conduction equation", *Numerical Heat Transfer, Part B: Fundamentals*, Vol. 44, No. 4, pp. 347-363, (2003).

[33] K. K. Tamma and S. B. Railkar, "Specially tailored transfinite element formulations for hyperbolic heat conduction involving non-Fourier effects", *Numerical Heat Transfer, Part B*, Vol. 15, No. 2, pp. 211-226, (1989).

[34] M. T. Manzari, "A mixed approach to finite element analysis of hyperbolic heat conduction problems", *International Journal of Numerical Methods for Heat &*

Fluid Flow, Vol. 8, No. 1, pp. 83-96, (1998)

[35] X. Ai, and B. Q. Li, "Discontinuous Finite Element Method for Non-Fourier Heat Conduction Problems", *Heat Transfer*, Vol. 1, No. 1, pp. 237-243,(2003).

[36] W. Wu, and X. Li, "Application of the time discontinuous Galerkin finite element method to heat wave simulation", *International Journal of Heat and Mass Transfer*, Vol. 49, No. 9-10, pp. 1679-1684, (2006).

[37] B. L. Wang, and J. C. Han, "A finite element method for non-Fourier heat conduction in strong thermal shock environments", *Front. Mater. Sci. China*, Vol. 4, No. 3, pp. 226-233, (2010).

[38] S. C. Mishra, T. B. Pavan Kumar, and B. Mondal, "Lattice Boltzmann Method Applied to the Solution of Energy Equation of a Radiation and Non-Fourier Heat Conduction Problem", *Numerical Heat Transfer A*, Vol. 54, No. 8, pp. 798-818, (2008).

[39] V. Vishwakarma, A. K. Das, and P. K. Das, "Analysis of non-Fourier heat conduction using smoothed particle hydrodynamics", *Applied Thermal Engineering*, Vol. 31, No. 14-15, pp. 2963-2970, (2011).

[40] J. Sladek, V. Sladek, C. L. Tan, and S. N. Atluri, "Analysis of transient heat conduction in 3D anisotropic functionally graded solids by the MLPG", *CMES*, Vol. 32, No. 3, pp. 161-174, (2008).

[41] X. H. Wu, and W. Q. Tao, "Meshless method based on the local weak-forms for steady-state heat conduction problems", *International Journal of Heat and Mass Transfer*, Vol. 51, No. 11-12, pp. 3103-3112, (2008).

[42] S. Soleimani, M. Jalaal, H. Bararnia, E. Ghasemi, D. D. Ganji, and F. Mohammadi, "Local RBF-DQ method for two-dimensional transient heat conduction problem", *International Communications in Heat and Mass Transfer*, Vol. 37, No. 9, pp. 1411-1418, (2010).

[43] Isa Ahmadi, and M. M. Aghdam, "Heat Transfer in Composite Materials using a New Truly Local Meshless Method", *International Journal of Numerical Methods for Heat and Fluid Flow*, Vol. 21, No. 3, pp. 293-309, (2011).

[44] S.N. Atluri and S. Shen, "The Meshless Local Petrov–Galerkin (MLPG) Method" Tech Science Press, Los Angeles, CA, (2002)

[45] D. Y. Tzou, J. K. Chen, "Thermal lagging in random media", *Journal of Thermophysics and Heat Transfer*, Vol. 12, No. 4, pp. 567-574, (1998).

[46] A. Moosaie, "Non-Fourier heat conduction in a finite medium with insulated boundaries and arbitrary initial conditions", *Int. Commun. Heat Mass Transfer*, Vol. 35, No. 1, pp. 103-111, (2008).